Chemistry Europe
European Chemical Societies Publishing
Batteries & Supercaps

RESEARCH ARTICLE OPEN ACCESS

Optimizing Conductive Networks in Metal Porphyrin Cathodes: A Path to High-Performance Alkali Metal-Ion Batteries

Masoumeh Zakerighadi[1] | Saibal Jana[1] | Ebrahim Abouzari-Lotf[2,3] | Svetlana Klyatskaya[1] | Dasari Bosubabu[2] | Wolfgang Wenzel[1] | Maximilian Fichtner[1,2] | Mario Ruben[1,4,5]

[1]Institute of Nanotechnology, Karlsruhe Institute of Technology, Eggenstein-Leopoldshafen, Germany | [2]Helmholtz Institute Ulm (HIU) Electrochemical Energy Storage, Ulm, Germany | [3]Trinseo Deutschland Anlagengesellschaft mbH, Rheinmünster, Germany | [4]Institute of Quantum Materials and Technologies (IQMT), Karlsruhe Institute of Technology, Eggenstein-Leopoldshafen, Germany | [5]Centre Européen de Science Quantique (CESQ) Institut de Science et d'Ingénierie Supramoléculaires (ISIS), Strasbourg Cedex, France

Correspondence: Ebrahim Abouzari-Lotf (eabouzarilotf@trinseo.com) | Mario Ruben (mario.ruben@kit.edu)

Received: 30 September 2025 | **Revised:** 19 March 2026 | **Accepted:** 23 March 2026

Keywords: conductive additives | graphene nanoplatelet | Li and Na-ion battery | organic electrode | porphyrinoids

ABSTRACT

Organic electrode materials (OEM)s have emerged as promising candidates for next-generation alkali metal-ion batteries due to their structural tunability, sustainability, and potential for high-rate capabilities. In this work, the role of conductive additives in tuning the electrochemical performance of a typical metal porphyrin-based organic cathode for lithium and sodium-ion batteries was investigated. By varying the type and content of conductive additives including graphene nanoplatelets (GNP), Ketjen black (KB), activated carbon (AC), and Super C (SC), the critical influence of conductive network architecture on capacity, rate capability and cycling stability was identified. Among them, GNP with planar morphology, enables efficient electronic pathways and delivers the highest capacities at low-to-moderate current densities, achieving up to 204 mAh g^{-1} in Li and 229 mAh g^{-1} in Na-ion cells at 100 mA g^{-1}. These findings have been elucidated by a combination of theoretical calculations, electrochemical impedance and extended cycling data. It is demonstrated that an optimal balance of conductive additive content and morphology is essential for long-term stability and high-rate performance. This study underscores the role of conductive additive and content in governing the charge transport kinetics of organic electrodes and provides valuable insights for designing high-performance electrode architectures in future sustainable energy storage systems.

1 | Introduction

The growing demand for sustainable and high-performance energy storage systems has intensified research into alternative redox active materials (AM) that can overcome the limitations of conventional lithium-ion batteries (LIBs). Although commercial LIBs are well placed in the market and dominate the current energy storage landscape—powering electric vehicles (EVs), portable electronics, and stationary storage systems—these technologies are largely dependent on inorganic, transition metal-based compounds. Such materials present challenges including high production costs, environmental concerns, uneven global resource distribution, and potential safety risks during operation [1, 2]. Among the alternatives redox AMs, organic electrode materials (OEMs) have gained great potential for sustainable charge storage devices not only as replacements for inorganic materials, but as options for niche applications due to their potential low cost, abundant resources, tunable performance, and environmental friendliness [3–5].

Despite the numerous advantages of OEMs [6], their practical application in rechargeable energy storage systems is hindered by four major challenges.

(i) A major drawback of OEMs is their substantial solubility in electrolytes, driven by strong solute–solvent interactions, polarity matching, hydrogen bonding, and dipole–dipole forces [2, 7, 8]. This dissolution results in the loss of redox-AMs, leading to progressive capacity fade. Additionally, the dissolved species can undergo undesirable side reactions with the counter electrode, further compromising battery performance.

(ii) The intrinsic poor conductivity of most OEMs hinders charge transport, increasing polarization and limiting active site utilization [9, 10]. While adding conductive additives (>40%) can partially facilitate the charge transfer, it also reduces overall energy density due to the added inactive mass.

(iii) The electrochemical potential of OEMs is typically below 3.0 V for cathodes or above 0.5 V for anodes, restricting the overall energy density [4].

(iv) OEMs inherently have a much lower density than conventional LIB cathodes. While their higher specific capacity can partially offset this drawback, it limits electrode loading, making it difficult to achieve comparable cell-level performance.

If the above challenges (i–iii) are addressed, OEMs could find practical niche applications where flexibility, sustainability, and low-cost materials are prioritized.

While the low density of OEMs is inherent, extensive research has focused on developing materials with higher redox potential [11], high capacity [5], and limited solubility [12]. Several reports highlight OEMs with acceptable cycling stability and electrochemical performance [13, 14].

Among the broad spectrum of organic redox-AMs, porphyrins represent a particularly promising class of OEMs. Their highly conjugated, planar macrocyclic structure facilitates efficient multielectron redox reactions, enabling high specific capacities [15–17]. A notable example is [5,15-bis-(ethynyl)-10,20-diphenylporphinato]copper(II) (or CuDEPP). CuDEPP combines a planar, π-rich structure with bipolar redox behavior (b-type), enabling reversible four-electron redox processes and high theoretical energy and power densities. Additionally, the introduction of acetylenic substituents reduces solubility in the electrolyte, while promoting in-situ electropolymerization upon cycling [18, 19]. Their redox-active cores and tunable peripheral substituents enable stable coordination with a wide range of cations, making them versatile platforms for high-performance and sustainable energy storage applications. Such metal-porphyrin derivatives have been successfully employed in a variety of monovalent and multivalent ion storage systems [20–25].

Despite these molecular advantages, CuDEPP suffers from poor electronic conductivity, which severely limits its practical electrochemical performance. To compensate, large amounts of conductive carbon are often added, which reduces energy density and complicates electrode fabrication [13]. The actual capacity of LIB electrodes depends not only on the redox-AM capacity but also on the optimization of electronic and ionic transport pathways [26–28]. While dense electrodes with high conductive carbon content promote electronic conduction via close particle–particle contact, high porosity and more AM fraction facilitate ionic diffusion and active sites, suggesting a tradeoff between the two. Therefore, enhancing charge transfer without compromising other key properties remains a significant challenge.

To overcome the limitations associated with the poor electronic conductivity of electrodes, the incorporation of modified conductive carbon additives is a widely adopted strategy, although predominantly explored in inorganic electrodes [29, 30]. While traditional additives such as carbon black (CB), Ketjen black (KB), Super C (SC), and activated carbon (AC) offer modest conductivity improvements, advanced carbon materials including carbon nanotubes (CNTs), graphene oxide (GO), and graphene nanoplatelets (GNPs) provide significantly enhanced electronic transport. Although CNTs can improve conductivity due to their high aspect ratio, their application is limited by high cost and difficulties in achieving homogeneous dispersion within electrode slurries [31, 32]. These limitations become even more pronounced in electrodes based on organic redox-AMs.

Among these, GNPs stand out as particularly promising due to their excellent structural integrity, high conductivity, and ease of dispersion. Unlike GO or reduced GO, GNPs are free of oxygen functional groups (OFGs), which helps preserve their sp^2 conjugated structure and results in significantly enhanced electronic conductivity, often several orders of magnitude higher [33–35]. Incorporating planar structures and extensive π-conjugation promotes π–π stacking, resulting in an ordered molecular arrangement that limits undesired solubility (of AMs) and enhances ion transport. Additionally, these intermolecular interactions can facilitate electron delocalization, thereby improving electrical conductivity [26]. While GNP and AC also contribute a small amount of pseudocapacitance or double-layer capacitance, their primary role in CuDEPP-based electrodes is to establish a conductive network. This work highlights the critical yet often underexplored role of conductive additive engineering in determining the electrochemical performance of porphyrin-based and other redox-active organic electrodes, emphasizing its importance as a key design parameter beyond AM engineering for enabling efficient organic electrode systems. In this study, we systematically investigate the influence of conductive additives in CuDEPP-based organic electrodes by comparing several carbon materials, including GNPs, and evaluate their electrochemical performance in both lithium- and sodium-ion systems, highlighting the efficiency of GNP in forming conductive networks.

2 | Results and Discussion

The electrochemical performance of CuDEPP electrodes is highly sensitive to the content of conductive carbon. As the AM relative content increases, resulting in a corresponding reduction in conductive additive, the discharge capacity significantly declines. As illustrated in Figure 1a, decreasing the conductive carbon content from 40% to 20% leads to a notable drop in capacity from 189 to 135 mAh g^{-1}, reflecting a ~30% reduction. The electrode formulation used here follows established recipes for metal porphyrins as reported in earlier literature [12, 19, 36]. This trend is consistent with previous observations in sodium-ion systems (Figure S1) [13].

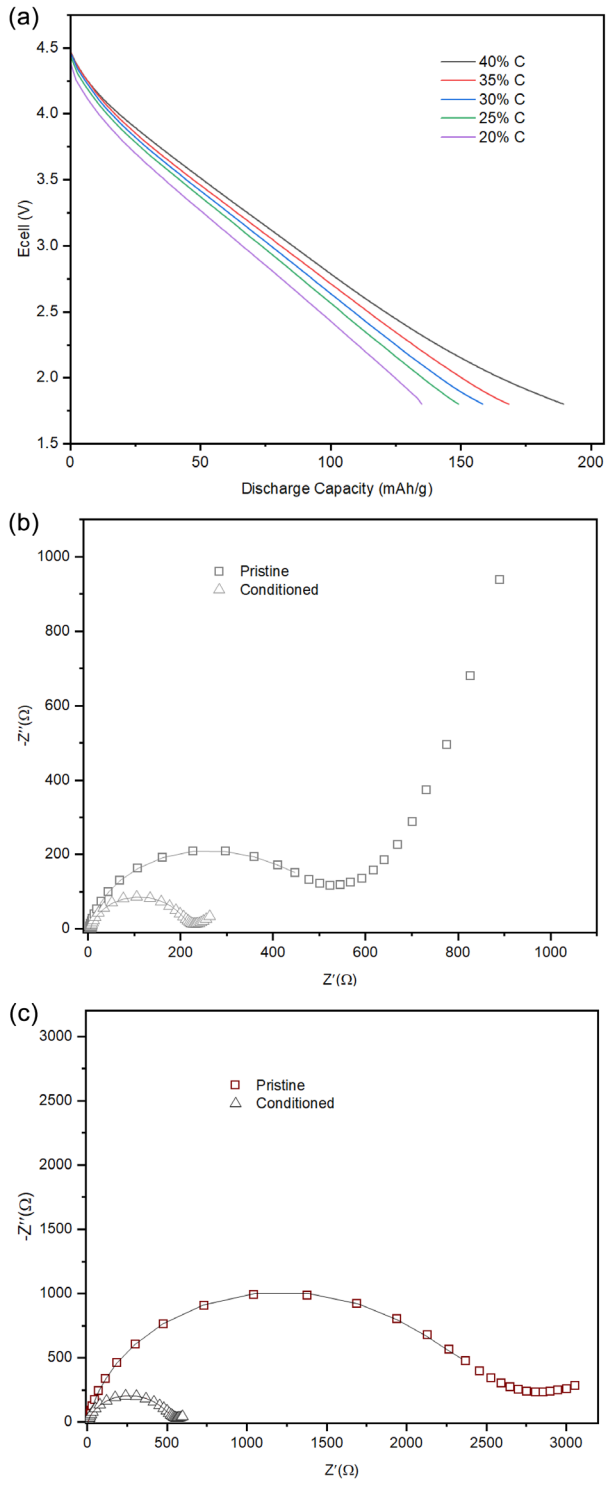

FIGURE 1 | (a) First discharge capacity of electrodes with varying conductive carbon contents at 100 mA g^{-1} in the potential range of 1.8–4.5 V in Li-ion cell. (b) EIS of electrodes with 40% conductive carbon and (c) 20% conductive carbon in fresh cells and after formation cycles.

To clarify the underlying reasons for this observation, Electrochemical impedance spectroscopy (EIS) measurements were conducted to compare the electrodes with 40% and 20% conductive carbon content in both fresh cells and after initial formation cycle. The Nyquist plots (Figure 1b,c) display a noticeable difference in the charge–transfer resistance (R_{ct}) between the two electrode formulations. The R_{ct}, identified as the diameter of the semicircle in the medium-frequency region, is an indicator of the charge transfer resistance to lithium insertion in anode. Additionally, the Warburg impedance, represented by the sloped line in the low-frequency region, reflects the difficulty of mass transport of the redox species to the CuDEPP electrode surface. The analysis shown that electrodes with higher conductive carbon content (40%) exhibited a significantly lower R_{ct}, approximately 4.8 times lower than that of the 20% carbon content electrodes. This difference is evident from the smaller semicircle in the high-frequency region of the impedance spectra, suggesting that enhanced electronic and ionic conductivity within the electrode matrix effectively reduces the energy barrier for charge transfer. Such a reduction in R_{ct} indicates more efficient ionic pathways, which is particularly advantageous under high-rate cycling conditions. Moreover, comparing the slopes of the straight line in the low-frequency region (Warburg impedance) revealed that electrodes with higher conductive carbon content exhibited a noticeably higher ion diffusion coefficient, indicating enhanced lithium-ion diffusion kinetics.

A similar trend was observed in the impedance spectra of electrodes after formation cycle, with approximately 105% higher charge transfer resistance in electrodes with lower conductive carbon content. Notably, the semicircles in the Nyquist plots became significantly smaller for both electrode types after the initial formation cycle, indicating a marked reduction in charge-transfer resistance compared to the pristine electrodes. This enhanced charge transfer efficiency after the formation cycle is likely due to a process often referred to as self-assembly [37, 38], self-conditioning [19], or polymerization of the rigid π-structures of the CuDEPP during the initial cycle operation [39]. The distinct irreversible oxidative peak observed in the first anodic sweep (Figure S2, CV, 1st cycle) provides clear evidence of this behavior, which appears to be a defining characteristic of this class of compounds. Similar phenomena have also been reported in related systems with Na^+ [13], K^+ [40] and Mg^{2+} [22] based chemistries, although a detailed discussion of the behavior is beyond the scope of this study.

To further understand the intrinsic electronic limitations of CuDEPP and its dependence on conductive carbon additives, first-principles density functional theory (DFT) calculations were performed to evaluate the electronic structure of the material. The goal was to elucidate the microscopic origin of charge transport limitations and assess how structural and electronic modifications can overcome these bottlenecks. Electronic conductivity in molecular materials is intimately linked to the electronic density of states (DOS) near the Fermi level. A finite DOS at the Fermi energy signifies the availability of mobile charge carriers and indicates metallic or conductive behavior. Conversely, the presence of a finite bandgap between the valence and conduction bands corresponds to semiconducting or insulating characteristics, depending on the gap magnitude.

Using the experimentally reported crystal structure of protected CuDEPP [19], full geometry optimization was performed, which confirmed its triclinic symmetry ($a = 6.282$ Å, $b = 9.140$ Å, $c = 11.892$ Å, $\alpha = 63.66°$, $\beta = 82.28°$, $\gamma = 82.11°$). The resulting DOS spectrum (Figure 2) revealed a bandgap of approximately 0.7 eV, indicative of a semiconducting character. Although relatively small, this bandgap still suggests limited intrinsic conductivity, consistent with the experimental observation that CuDEPP

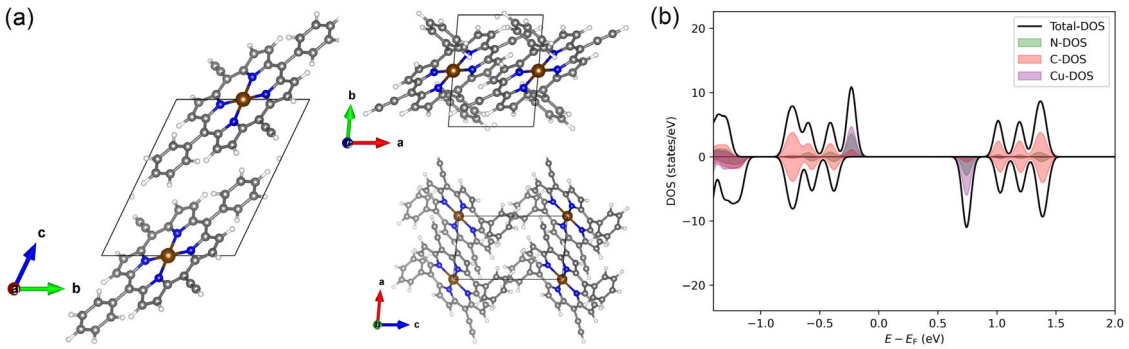

FIGURE 2 | (a) Crystal structure of CuDEPP in its triclinic phase, visualized from multiple orientations to highlight the unit cell geometry and molecular packing. (b) Total and element-resolved projected density of states (PDOS) for CuDEPP. The Fermi level is aligned to 0 eV. The calculated bandgap is approximately 0.7 eV, indicating semiconducting behavior. Colored shades represent the contributions from individual atomic species to the electronic states.

requires substantial conductive additive content for optimal performance.

To enhance electronic conductivity, the incorporation of conductive carbon additives has been commonly utilized as an experimental strategy. However, conventional conductive additives such as carbon black or acetylene black are typically amorphous, leading to limited and less predictable electronic interaction with crystalline OEMs due to reduced interfacial contact and challenges in modeling. Instead, we focused on GNPs-a crystalline, two-dimensional carbon material with high specific surface area and superior electrical properties-as a more effective and structurally compatible additive for layered molecular systems.

Given the low-symmetry nature of CuDEPP and its layered morphology, the [2 −3 3] crystallographic plane was identified as the most representative surface for interfacial interaction with GNPs. A series of CuDEPP-GNP heterojunction models (two-layer of CuDEPP and single layer of GNP) was constructed, and the interlayer spacing was systematically varied by 0.1 Å to probe the influence of proximity on electronic coupling. As shown in Figure S3, the interfacial interaction energy was maximized at an optimal interplanar distance of 3.9 Å.

Considering the structure with optimal interplanar distance of the CuDEPP-GNP composite, the projected density of states (PDOS) was computed to investigate the electronic hybridization between the organic framework and GNPs. The analysis (see Figure 3) demonstrates a clear emergence of continuous electronic states at and around the Fermi level, indicative of delocalized charge carriers and a transition toward metallic behavior. This significant increase in the DOS at the Fermi energy highlights the enhanced electronic conductivity of the composite system. These findings suggest that GNPs, owing to their extended π-conjugated structure and favorable crystallographic matching, serve as a superior conductive additive for CuDEPP-based organic electrodes. The enhanced charge transport at the CuDEPP–GNP interface is thus expected to translate into improved electron mobility and overall electrode performance.

Furthermore, the superior charge transport properties inferred from the PDOS analysis are confirmed by experimental measurements of composite volume resistivity. Specifically, the CuDEPP-GNP electrode exhibited a composite volume resistivity of 0.449 Ω.cm, which is significantly lower than that of corresponding electrodes incorporating conventional carbon blacks

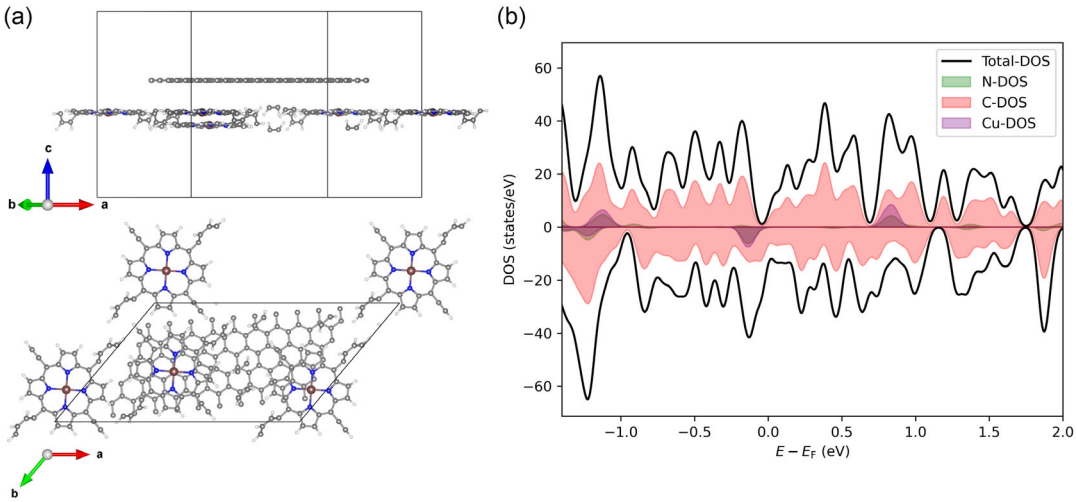

FIGURE 3 | (a) The atomic structure of the CuDEPP–GNP heterojunction at an interlayer distance of 3.9 Å, viewed from multiple orientations to emphasize unit cell geometry, stacking arrangement, and interfacial alignment. (b) Total and atom-PDOS for the CuDEPP–GNP composite. The Fermi level is set to 0 eV. The presence of continuous electronic states at the Fermi level indicates a metallic character of the heterostructure. Colored regions represent the contributions from individual atomic species to the electronic structure.

(2.102 Ω.cm). The combination of intrinsic GNP conductivity and intimate interfacial contact with CuDEPP molecules likely facilitates more efficient charge delocalization and electron transport, thus reinforcing the role of GNPs as a highly efficient conductive additive for planar porphyrin electrodes.

In a parallel study, we examined another organic cathode material, crystalline 3,4,9,10-perylenetetracarboxylic dianhydride (PTCDA) [41], with a smaller bandgap (~0.5 eV) compared to CuDEPP, which has been extensively investigated for its redox-active and planar π-conjugated structure (Figure S4) [41]. Electronic structure calculations revealed, that, upon interfacing with GNPs, this material exhibits a significant increase in electron density near the Fermi level. However, a subtle discontinuity was observed in the conduction band region (Figure 4). This suggests that, although the intrinsic electronic conductivity of the PTCDA is superior to that of pristine CuDEPP, its performance does not exceed that of the CuDEPP–GNP heterostructure when interfacial interactions with GNPs are considered. This demonstrates that the remarkable electronic enhancement in CuDEPP–GNP arises from a unique and favorable interfacial interaction, rather than being a consequence of GNP incorporation in organic cathodes.

To experimentally validate the effectiveness of GNP as a conductive additive, its performance was systematically studied and compared with other commonly used carbon materials. Specifically, CuDEPP electrodes incorporating KB, AC, SC, GNP, and a GNP/SC composite (10% GNP/20% SC) were fabricated and evaluated under identical conditions to assess their influence on electrochemical performance. Meanwhile, during this study, it was also noted that a relatively high binder content (10%) had been used in earlier reports, which might not be necessary for maintaining adequate electrode integrity. This observation has initiated a parallel investigation to find optimal binder content. To this end, the binder ratio was reduced from 10 parts to 7 and 5.5 parts out of 100 total parts of the electrode composition, while keeping the ratios of conductive carbon and AM constant. Notably, this reduction did not result in any measurable decline in peel adhesion. Peel tests showed that the adhesion strength remained consistent at approximately 1.1–1.4 N m^{-1} across all formulations, indicating that mechanical integrity was preserved despite the lower binder content. These findings suggest that a binder content of 5.5 parts is sufficient to ensure good slurry processing and robust peel adhesion with all conductive carbon additives investigated here, potentially enhancing overall electrochemical performance by reducing inactive mass without compromising structural stability. Accordingly, all subsequent electrode compositions were standardized at 5.5% binder, 30% conductive carbon, and 64.5% CuDEPP AM. The morphology of the composite electrodes was examined using SEM (Figure 5), revealing a uniform dispersion of pristine CuDEPP particles and conductive carbons (Figure S5) across all samples, regardless of the conductive additive used.

However, variations in the electrode microstructure were evident depending on the type of conductive additive. GNP, with its planar, sheet-like structure (Figure S5a), appeared to form a more continuous and efficient conductive network. This may result from the planar structure of GNP, which reduces agglomeration compared to spherical carbon additives. Similar advantages have been observed in LFP cathodes, where graphene-based conductive additives act as buffers, improving the dispersion of active particles [42]. The point-contact nature of the other additives with the AM restricts electron transfer, likely contributing to lower electronic conductivity.

Electrochemical performance was evaluated by cycling the electrodes between 4.5 and 1.8 V versus Li^+/Li at a current density of 0.1 A g^{-1}. The discharge profiles, shown in Figure 6a, exhibit sloped voltage curves without distinct plateaus, suggesting rapid pseudocapacitive redox reactions. This behavior is attributed to a combination of double-layer capacitance and multiple redox reactions, a characteristic commonly observed in such organic electrodes [43]. The first-cycle discharge capacities of the CuDEPP electrodes followed the order: CuDEPP-GN*P* > CuDEPP-AC > CuDEPP-SC > CuDEPP-KB > CuDEPP-GNP/SC, with values of 194, 178, 175, 170, and 142 mAh g^{-1}, respectively. As expected, CuDEPP-GNP exhibited the highest discharge capacity, indicating that GNP enhances both conductivity and structural connectivity

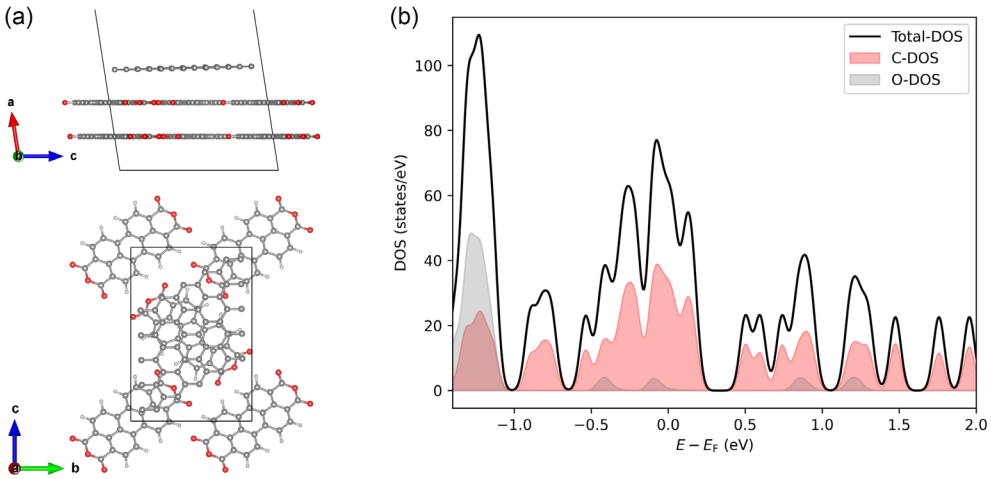

FIGURE 4 | (a) The atomic structure of the PTCDA-GNP heterojunction at an interlayer distance of 3.7 Å, viewed from two-different orientations to emphasize unit cell geometry, stacking arrangement, and interfacial alignment. (b) Total and atom-PDOS for the PTCDA–GNP composite. The Fermi level is set to 0 eV. The presence of continuous electronic states at the Fermi level indicates a metallic character of the heterostructure, though a subtle discontinuity is present in the conduction band. Colored regions represent the contributions from individual atomic species to the electronic structure.

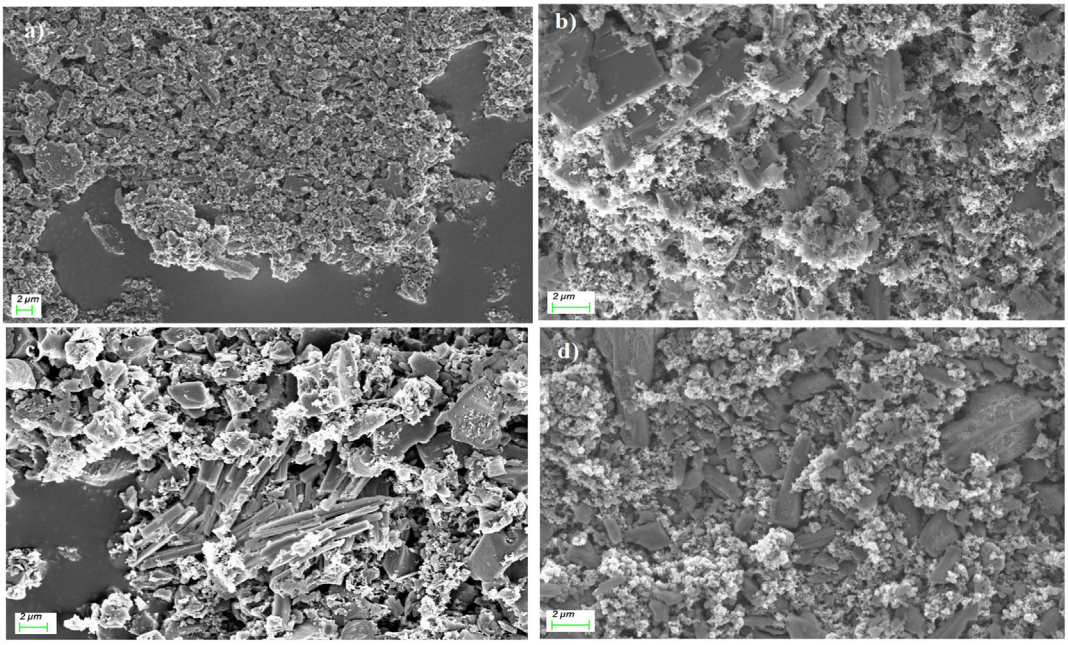

FIGURE 5 | The SEM images of CuDEPP-based electrodes with various conductive additives: (a) GNP, (b) SC, (c) AC and (d) KB.

within the electrode. This superior performance can be attributed to the continuous electronic states at the Fermi level and the efficient charge transport pathways enabled by the strong interfacial interaction between CuDEPP and the planar, conductive GNP network. Interestingly, although hybrid graphene–CB conductive networks have been reported to enhance electronic percolation in some inorganic cathodes [44], the expected synergistic effect was not observed here, suggesting that SC may disrupt the planar conductive pathways provided by GNP in the CuDEPP electrode.

The rate performance was evaluated at current densities ranging from 0.1 to 12 A g^{-1}, with each rate maintained for 20 cycles (as shown in Figure 6b). The corresponding oulombic efficiencies are provided in the Supporting Information (Figures S6–S10). This range includes the typical rates utilized in LIBs, extending to extremely fast charging conditions. At a low current density of 0.1 A g^{-1}, all electrodes except CuDEPP-GNP/SC exhibit similar performance, with CuDEPP-GNP showing the highest discharge capacity of 204 mAh g^{-1} after 20 cycles. CuDEPP-AC demonstrates a gradual increase in capacity over the first 20 cycles, stabilizing at a value comparable to CuDEPP-GNP. In contrast, CuDEPP-SC and CuDEPP-KB show lower discharge capacities, remaining at a similar level. As the current density increases, distinct differences in rate capability and capacity retention emerge. Up to 2 A g^{-1}, CuDEPP–GNP maintains the highest discharge capacity and demonstrates the best rate capability. Representative charge–discharge profiles of CuDEPP-GNP at different current densities are shown in Figure 6c. Even at a higher current density of 4 A g^{-1}, the capacity remained at 134 mAh g^{-1} indicating efficient charge transport. After 200 cycles, the cell regained a capacity of 177 mAh g^{-1}, also demonstrating good stability. This indicates that CuDEPP–GNP provides efficient stability during cycling at various rates. At 4 A g^{-1}, CuDEPP-KB slightly outperforms CuDEPP–GNP, while CuDEPP–AC exhibits a significant decline in capacity, which is further declined at 8 and 12 A g^{-1}. At high current densities of 8 and 12 A g^{-1}, SC exhibits higher discharge capacity.

The lower rate capability of CuDEPP–AC can be attributed to the predominantly microporous structure of AC (pore size typically <2 nm). While its high surface area can enhance charge storage at low current densities, ion transport within micropores becomes increasingly diffusion-limited under fast cycling conditions, leading to increased polarization and reduced capacity at high rates [45, 46].

The observed rate-dependent performance differences can be understood in terms of electronic and ionic transport limitations in the electrodes [26]. At low to medium current densities, where charge transport is not severely limited, electronic conductivity plays a dominant role in enabling efficient electron flow, resulting in higher capacity. This explains why CuDEPP–GNP, with its planar and highly conductive structure, achieves superior performance in such rates. However, as the current density increases, ionic conductivity becomes the primary limiting factor since fast ion diffusion is required to sustain charge storage. At extreme high rates, the small particle size and isotropic morphology of SC may shorten ion diffusion pathways. In contrast, the stacked lamellar architecture of GNP, despite its high surface area, could introduce tortuous ion transport pathways and impede the performance at very high-rate performance [47].

Unlike inorganic cathode materials, OEMs offer greater structural flexibility, making them highly compatible across different alkali metal-ion battery systems. To further explore the advantages of planner conductive additive, the electrochemical performance of CuDEPP–GNP electrodes was evaluated as the cathode in a Na half-cell configuration. As shown in Figure 7a, electrodes with GNP exhibited significantly higher capacity compared to previously reported electrodes with CB (Figure S1) and the reference cell using SC as the conductive additive (Figure S11) [13, 19].

We have also investigated the influence of GNP content on the electrochemical performance of CuDEPP-GNP electrodes in Na-ion cells. Thus, three different electrodes with 30 wt%, 25 wt%, and 15 wt% of GNP were prepared to fully demonstrate their

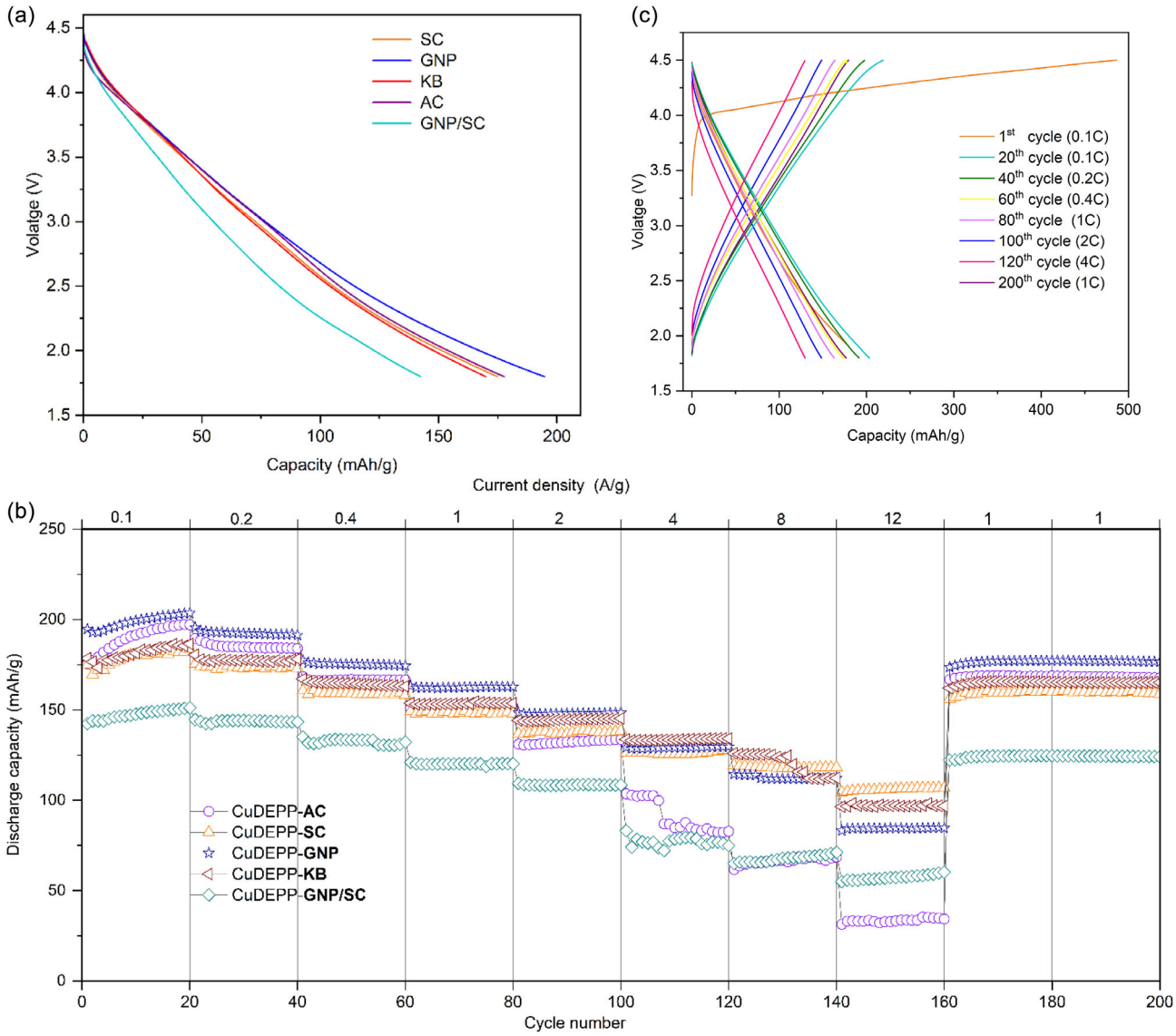

FIGURE 6 | (a) Initial discharge curves of CuDEPP cathodes at 0.1 A g^{-1}. (b) Rate capability of CuDEPP electrodes with different conductive additives in rates 0.1, 0.2, 0.4, 1, 2, 4, 8, and 12 A g^{-1}. (c) Selected charge–discharge curves of CuDEPP-GNP at different cycles. All electrodes contained 30% conductive additive, 5.5% binder, and 64.5% CuDEPP active material.

energy storage performance, named GNP-30, GNP-25, and GNP-15, respectively. The results indicate that the electrode with higher GNP content delivered higher capacity (Figure 7a). At a relatively low current density of 0.1 A g^{-1}, the discharge capacities increased with cycle number. Specifically, GNP-30 exhibited an initial discharge capacity of 207 mAh g^{-1} (Figure S12), which further increased to 229 mAh g^{-1} by the 20th cycle. The rate capability of the three different cells was also evaluated at different current densities (Figure 7b). At 0.1 A g^{-1}, the highest initial discharge capacity was observed for GNP-30 (229 mAh g^{-1}), followed by GNP-25 (194 mAh g^{-1}) and GNP-15 (148 mAh g^{-1}). As the current density increased, a gradual capacity fade was observed for all electrodes. However, GNP-30 consistently retained the highest capacity across all rates, maintaining a discharge capacity of 151 mAh g^{-1} even at 4 A g^{-1}, suggesting superior rate performance and efficient charge transport. As shown in Figure S13, the coulombic efficiency rises above 95% within the initial cycles and stabilizes at around 99%–100% upon extended cycling. GNP-30 delivers reversible capacities of 206, 194, 177, 149, 130 and 106 mAh g^{-1} at current densities of 0.4, 1, 2, 4, 8, and 12 A g^{-1}, respectively (Figure S14).

After the rate tests, the cycling of the cells continued for another 340 cycles at 1 A g^{-1} (Figure S15). Even after 500 cycles, GNP-30 maintained a reversible capacity of 194 mAh g^{-1}, corresponded to 98% of the initial values at current density of 1 A g^{-1}. Similarly, GNP-25 retained 95% of its capacity with176 mAh g^{-1} after 500 cycles. This exceptional cycling stability was further confirmed by the well-overlapped charge–discharge curves of GNP-30 at cycles 50–300, highlighting minimal polarization and highly reversible capability (Figure 7c).

Comparing rate-dependent capacity based on the total electrode mass, rather than normalizing to AM alone, provides a more realistic view of the practical advantages gained through conductive carbon optimization. Figure 7d presents such a comparison between CuDEPP–GNP and previously reported CuDEPP–CB electrodes. As shown, the CuDEPP–GNP system exhibits

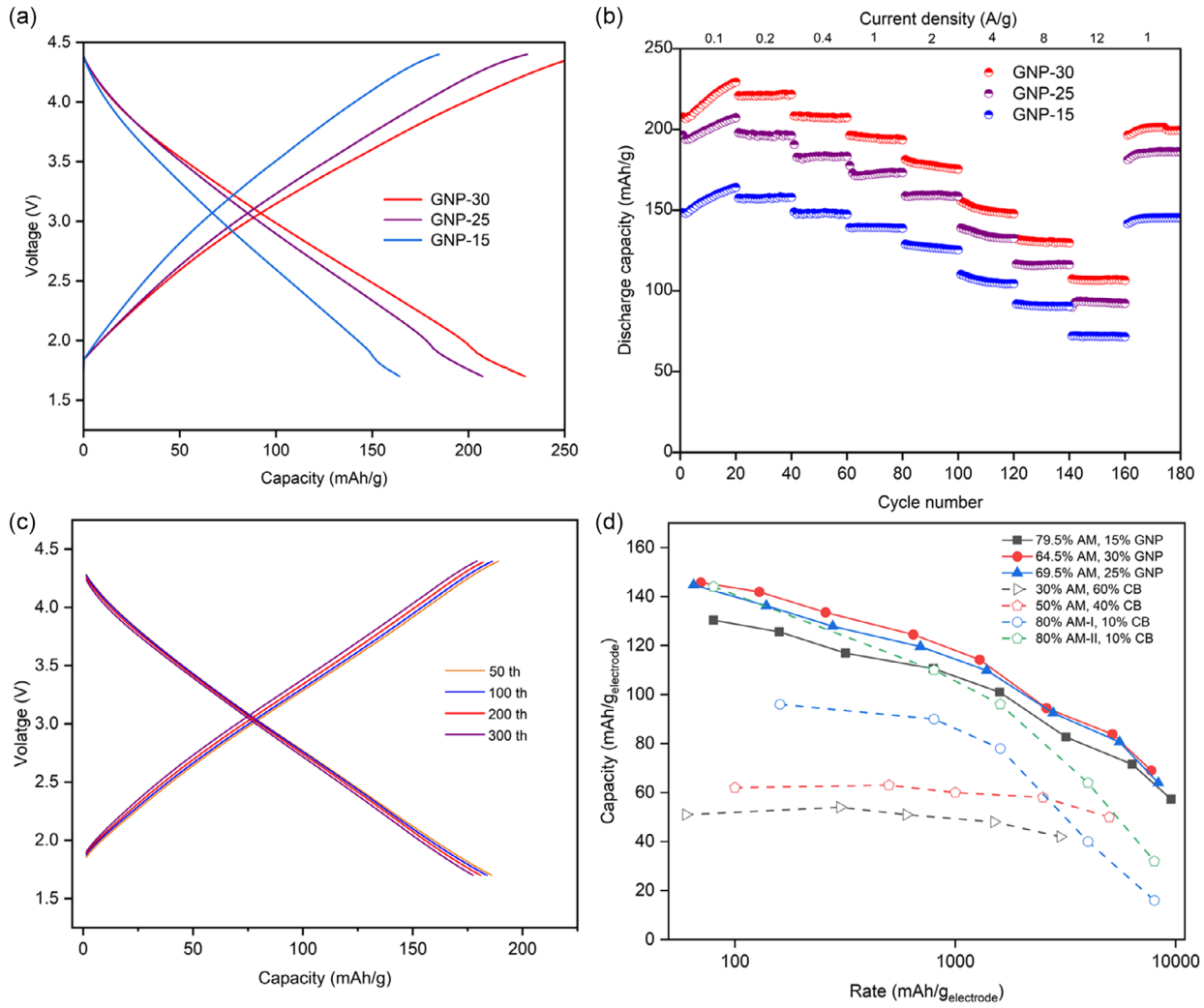

FIGURE 7 | (a) Comparative charge–discharge curves of GNP-30, 25, 15 electrodes at 0.1 A g^{-1} in Na-ion battery (20th cycle). (b) Rate capability of CuDEPP electrodes with different content of GNP in rates 0.1, 0.2, 0.4, 1, 2, 4, 8, and 12 A g^{-1} in Na-ion cells. (c) Selected charge–discharge curves of GNP-30 at 1 A g^{-1} (after the rate test). (d) Rate-dependent capacity comparison based on total electrode mass for CuDEPP–GNP versus CuDEPP–CB (data for CuDEPP–CB were adapted and replotted from Ref [13] under CC BY 4.0.).

improved performance across rates, highlighting the impact of conductive network engineering.

3 | Conclusion

This work presents a systematic evaluation of various conductive carbon additives for CuDEPP-based organic cathodes in both lithium-ion and sodium-ion cells, addressing a critical limitation of organic AMs: their inherently low electrical conductivity. Among the tested materials, GNPs emerged as the most effective conductive additive. Their high electrical conductivity and planar morphology enable superior charge percolation networks that led to a remarkable 75% reduction in bulk electrode resistivity. Electronic structure analysis revealed the emergence of delocalized electronic states near the Fermi level in the CuDEPP–GNP composite, indicating a transition toward metallic-like conductivity. This enhanced electronic hybridization, driven by the extended π-conjugation and crystallographic compatibility of GNPs, facilitates superior charge transport at the electrode interface, contributing directly to the improved performance observed in both lithium- and sodium-ion cells. The CuDEPP-GNP composite electrodes demonstrated significantly enhanced electrochemical performance in both sodium-ion and lithium-ion cells. Specifically, electrode with 30 wt% GNP (GNP-30), exhibited outstanding electrochemical performance, achieving high capacities and exceptional cycling stability. The energy and power performance of the GNP-based CuDEPP cathode was also notable in sodium ion cells. At 0.1 A g^{-1}, with an average discharge voltage of 2.8 V, the gravimetric energy density reached approximately 641 Wh kg^{-1} (based on AM). Even at an extreme rate of 8 A g^{-1}, it maintained an energy density of 338 Wh kg^{-1} and a power density of 20.8 kW kg^{-1}. This work highlights the critical yet often underexplored role of conductive additive engineering to unlock the performance potential of not only CuDEPP, but a broad class of porphyrin-based and other redox-active organic electrodes.

Acknowledgments

This work contributes to the research performed at CELEST (Center for Electrochemical Energy Storage Ulm-Karlsruhe) and was funded by the

German Research Foundation (DFG) under Project ID 390874152 (POLiS Cluster of Excellence). The work was partly carried out with the support of the Karlsruhe Nano Micro Facility (KNMF, http://www.knmf.kit.edu), a Helmholtz Research Infrastructure at Karlsruhe Institute of Technology (KIT, http://www.kit.edu). The authors acknowledge support with computational resources provided by the state of Baden-Württemberg through bwHPC (bwForCluster JUSTUS).

Open Access funding enabled and organized by Projekt DEAL.

Funding

This study was supported by (390874152).

Conflicts of Interest

The authors declare no conflicts of interest.

Data Availability Statement

The data that support the findings of this study are available from the corresponding author upon reasonable request.

References

1. Q. Wang, T. O'Carroll, F. Shi, et al., "Designing Organic Material Electrodes for Lithium-Ion Batteries: Progress, Challenges, and Perspectives," *Electrochemical Energy Reviews* 7 (2024): 15.

2. Y. Lu and J. Chen, "Prospects of Organic Electrode Materials for Practical Lithium Batteries," *Nature Reviews Chemistry* 4 (2020): 127–142.

3. J. Bitenc, K. Pirnat, O. Lužanin, and R. Dominko, "Organic Cathodes, a Path toward Future Sustainable Batteries: Mirage or Realistic Future?," *Chemistry of Materials* 36 (2024): 1025–1040.

4. Z. Wu, Q. Liu, P. Yang, et al., "Molecular and Morphological Engineering of Organic Electrode Materials for Electrochemical Energy Storage," *Electrochemical Energy Reviews* 5 (2022): 26.

5. A. Banerjee, N. Khossossi, W. Luo, and R. Ahuja, "Promise and Reality of Organic Electrodes from Materials Design and Charge Storage Perspective," *Journal of Materials Chemistry A* 10 (2022): 15215–15234.

6. M. R. Raj, G. Lee, M. V. Reddy, and K. Zaghib, "Recent Advances in Development of Organic Battery Materials for Monovalent and Multivalent Metal-Ion Rechargeable Batteries," *ACS Applied Energy Materials* 7 (2024): 8196–8255.

7. C. Cong and H. Ma, "Advances of Electroactive Metal-Organic Frameworks," *Small* 19 (2023): e2207547.

8. Y. Shi, J. Yang, J. Yang, Z. Wang, Z. Chen, and Y. Xu, "Quinone-Amine Polymer Nanoparticles Prepared through Facile Precipitation Polymerization as Ultrafast and Ultralong Cycle Life Cathode Materials for Lithium-Ion Batteries," *Advanced Functional Materials* 32 (2022): 2111307.

9. X. Jia, Y. Ge, L. Shao, C. Wang, and G. G. Wallace, "Tunable Conducting Polymers: Toward Sustainable and Versatile Batteries," *ACS Sustainable Chemistry and Engineering* 7 (2019): 14321–14340.

10. C. Hwang, J. Lee, J. Jeong, et al., "The Rational Design of a Redox-Active Mixed Ion/Electron Conductor as a Multi-Functional Binder for Lithium-Ion Batteries," *Journal of Materials Chemistry A* 9 (2021): 4751–4757.

11. R. Shi, S. Jiao, Q. Yue, G. Gu, K. Zhang, and Y. Zhao, "Challenges and Advances of Organic Electrode Materials for Sustainable Secondary Batteries," *Exploration* 2 (2022): 20220066.

12. X. Peng, Y. Zhou, B. Chen, et al., "A Porphyrin-Phenylalkynyl-Based Conjugated Organic Polymer as a High-Performance Cathode for Rechargeable Organic Batteries," *ACS Applied Materials and Interfaces* 16 (2024): 55511–55519.

13. X. Chen, X. Feng, B. Ren, et al., "High Rate and Long Lifespan Sodium-Organic Batteries Using Pseudocapacitive Porphyrin Complexes-Based Cathode," *Nano-Micro Letters* 13 (2021): 71.

14. J. Wang, H. Yao, C. Du, and S. Guan, "Polyimide Schiff Base as a High-Performance Anode Material for Lithium-Ion Batteries," *Journal of Power Sources* 482 (2021): 228931.

15. S. Chowdhury, S. Jana, S. P. K. Panguluri, W. Wenzel, S. Klayatskaya, and M. Ruben, "Ferrocene Appended Porphyrin-Based Bipolar Electrode Material for High-Performance Energy Storage," *ChemSusChem* 17 (2024): e202301903.

16. J. Zhang, C. Ye, Y. Zhou, et al., "An Extended Thiophene Chain for Ni-Based Porphyrin Derivatives Enabling a High Potential and Long Cycle Life for Electrochemical Charge Storage," *Journal of Materials Chemistry A* 12 (2024): 22809–22819.

17. J. Gu, Y. Peng, T. Zhou, J. Ma, H. Pang, and Y. Yamauchi, "Porphyrin-Based Framework Materials for Energy Conversion," *Nano Research Energy* 1 (2022): e9120009.

18. S. Chowdhury, S. Jana, S. Klyatskaya, and M. Ruben, "A Bithiophene-Substituted Porphyrin Displaying Multi-Electron Redox Processes as a Cathode for Lithium Organic Batteries," *Journal of Porphyrins and Phthalocyanines* 28 (2024): 253–259.

19. P. Gao, Z. Chen, Z. Zhao-Karger, et al., "A Porphyrin Complex as a Self-Conditioned Electrode Material for High-Performance Energy Storage," *Angewandte Chemie International Edition* 56 (2017): 10341–10346.

20. T. Smok, S. Shakouri, E. Abouzari-Lotf, et al., "A π-Conjugated Porphyrin Complex as Cathode Material Allows Fast and Stable Energy Storage in Calcium Batteries," *Batteries and Supercaps* 6 (2023).

21. S. Chowdhury, N. Sabi, R. C. Rojano, et al., "π-Conjugated Metal Free Porphyrin as Organic Cathode for Aluminum Batteries," *Batteries and Supercaps* 7 (2024): e202300285.

22. E. Abouzari-Lotf, R. Azmi, Z. Li, et al., "A Self-Conditioned Metalloporphyrin as a Highly Stable Cathode for Fast Rechargeable Magnesium Batteries," *ChemSusChem* 14 (2021): 1840–1846.

23. S. Lv, J. Yuan, Z. Chen, et al., "Copper Porphyrin as a Stable Cathode for High-Performance Rechargeable Potassium Organic Batteries," *ChemSusChem* 13 (2020): 2286–2294.

24. X. Peng, B. Ren, C. Sun, et al., "Ultra-Long Lifespan Ni Based Porphyrin Complex Cathode for Organic Alkali Metal Batteries," *Batteries and Supercaps* 7 (2024): e202400031.

25. Y. Guo, W. Wang, K. Guo, et al., "A Bipolar-Redox Tetraalkynylporphyrin Macrocycle Positive Electrode with 12-Electrons-Transfer for High-Energy Aluminum-Organic Batteries," *Nature Communications* 16 (2025): 2794.

26. M. Zhuo, D. Grazioli, and A. Simone, "Active Material Utilization and Capacity of Fiber-Based Battery Electrodes," *Electrochimica Acta* 333 (2020): 134929.

27. Y. H. Chen, C. W. Wang, X. Zhang, and A. M. Sastry, "Porous Cathode Optimization for Lithium Cells: Ionic and Electronic Conductivity, Capacity, and Selection of Materials," *Journal of Power Sources* 195 (2010): 2851–2862.

28. H. Zheng, R. Yang, G. Liu, X. Song, and V. S. Battaglia, "Cooperation between Active Material, Polymeric Binder and Conductive Carbon Additive in Lithium Ion Battery Cathode," *Journal of Physical Chemistry C* 116 (2012): 4875–4882.

29. S. Xue, J. Wang, Y. Xia, et al., "Mesoporous Carbon as Conductive Additive to Improve the High-Rate Charge/Discharge Capacity of Lithium-Ion Batteries," *Energy Technology* 10 (2022): 2200472.

30. J. Geng, S. Zhang, X. Hu, et al., "A Review of Graphene-Decorated $LiFePO_4$ Cathode Materials for Lithium-Ion Batteries," *Ionics* 28 (2022): 4899–4922.

31. F.-Y. Su, C. You, Y.-B. He, et al., "Flexible and Planar Graphene Conductive Additives for Lithium-Ion Batteries," *Journal of Materials Chemistry* 20 (2010): 9644–9650.

32. E. Muchuweni, E. T. Mombeshora, C. M. Muiva, and T. S. Sathiaraj, "Lithium-Ion Batteries: Recent Progress in Improving the Cycling and Rate Performances of Transition Metal Oxide Anodes by Incorporating Graphene-Based Materials," *Journal of Energy Storage* 73 (2023): 109013.

33. A. A. Adepoju, M. Doumbia, and Q. L. Williams, "Graphene Nanoplatelet Additives for High C-Rate $LiFePO_4$ Battery Cathodes," *JOM* 72 (2020): 3170–3175.

34. I. Esteve-Adell, M. Porcel-Valenzuela, L. Zubizarreta, M. Gil-Agustí, M. García-Pellicer, and A. Quijano-Lopez, "Influence of the Specific Surface Area of Graphene Nanoplatelets on the Capacity of Lithium-Ion Batteries," *Frontiers in Chemistry* 10 (2022).

35. Y. Han, Z. Liu, F. Zheng, et al., "Two-Dimensional Flower-Like Cobalt-Porphyrin MOF/rGO Composite Anodes for High-Performance Li-Ion Batteries," *Journal of Alloys and Compounds* 881 (2021): 160531.

36. J. Zhou, B. Zheng, X. Huang, et al., "High Voltage, Long Cycling Organic Cathodes Rendered by In Situ Electrochemical Oxidation Polymerization," *Advanced Functional Materials* 34 (2024): 2411127.

37. S. Shakouri, E. Abouzari-Lotf, J. Chen, et al., "Molecular Engineering of Metalloporphyrins for High-Performance Energy Storage: Central Metal Matters," *ChemSusChem* 16 (2023): e202202090.

38. Y. Zhao, J. Wang, and R. Pei, "Micron-Sized Ultrathin Metal–Organic Framework Sheet," *Journal of the American Chemical Society* 142 (2020): 10331–10336.

39. T. Philipp, G. Neusser, E. Abouzari-Lotf, et al., "Visualization of Structural Changes and Degradation of Porphyrin-Based Battery Electrodes," *Journal of Power Sources* 522 (2022): 231002.

40. Z. Chen, P. Gao, W. Wang, et al., "A Lithium-Free Energy-Storage Device Based on an Alkyne-Substituted-Porphyrin Complex," *ChemSusChem* 12 (2019): 3737–3741.

41. I. A. Rodríguez-Pérez, Y. Yuan, C. Bommier, et al., "Mg-Ion Battery Electrode: An Organic Solid's Herringbone Structure Squeezed upon Mg-Ion Insertion," *Journal of the American Chemical Society* 139 (2017): 13031–13037.

42. E. Muchuweni, E. T. Mombeshora, C. M. Muiva, and T. S. Sathiaraj, "Towards High-Performance Lithium-Ion Batteries by Introducing Graphene-Based Materials into $LiFePO_4$ Cathodes: A Review," *Nano Trends* 6 (2024): 100034.

43. J. Yuan, B. Ren, X. Feng, P. Gao, E. Liu, and S. Tan, "A Coupled Polymeric Porphyrin Complex as a Novel Cathode for Highly Stable Lithium Organic Batteries," *Chemical Communications* 56 (2020): 5437–5440.

44. T. Liu, S. Sun, Z. Zang, et al., "Effects of Graphene with Different Sizes as Conductive Additives on the Electrochemical Performance of a $LiFePO_4$ Cathode," *RSC Advances* 7 (2017): 20882–20887.

45. K. Zou, P. Cai, X. Cao, G. Zou, H. Hou, and X. Ji, "Carbon Materials for High-Performance Lithium-Ion Capacitor," *Current Opinion in Electrochemistry* 21 (2020): 31–39.

46. F. Béguin, V. Presser, A. Balducci, and E. Frackowiak, "Carbons and Electrolytes for Advanced Supercapacitors," *Advanced Materials* 26 (2014): 2219–2251.

47. V. Nemani, S. Harris, and K. Smith, "Design of Bi-Tortuous, Anisotropic Graphite Anodes for Fast Ion-Transport in Li-Ion Batteries," *Journal of the Electrochemical Society* 162 (2015): A1415–A1423.

Supporting Information

Additional supporting information can be found online in the Supporting Information section.